Supporting Information

Transition Metal Dichalcogenides Magnetic Atomic Chains

Kai Zhang,[1] Xiaojun Wu[1,2,*], and Jinlong Yang[1,2]

[1] Hefei National Research Center for Physical Sciences at the Microscale, University of Science and Technology of China, Hefei, Anhui 230026, China

[2] School of Chemistry and Materials Sciences, CAS Key Lab of Materials for Energy Conversion, Synergetic Innovation of Quantum Information & Quantum Technology, and CAS Center for Excellence in Nanoscience, University of Science and Technology of China, Hefei, Anhui 230026, China

* Corresponding Email Address: xjwu@ustc.edu.cn

Table of Contents

Table S1. The calculated relative energies (eV/metal) of transition metal dichalcogenides (TMD) chains with different configurations.

Chain	A	Z	S	T	C	Chain	A	Z	S	T	C
TiS_2	1.34	0.62	1.40	0	2.62	**FeS_2**	0.65	0.22	0.64	0	1.59
$TiSe_2$	1.18	0.97	1.20	0	2.08	**$FeSe_2$**	0.36	0.12	0.37	0	1.15
$TiTe_2$	0.86	0.18	0.86	0	1.35	**$FeTe_2$**	0.28	0	0.36	0.14	0.77
VS_2	1.30	0.90	1.29	0	2.59	**ScS_2**	1.30	0	1.30	0.92	2.18
VSe_2	1.04	0.68	1.04	0	2.15	**$ScSe_2$**	1.20	0	1.01	0.82	2.00
VTe_2	0.79	0.18	0.76	0	1.52	**$ScTe_2$**	0.60	0	0.21	0.28	1.34
CrS_2	1.84	0.66	1.10	0	2.11	**CoS_2**	0.81	0	0.70	0.24	0.55
$CrSe_2$	1.55	0.65	0.79	0	1.41	**$CoSe_2$**	0.45	0	0.49	0.21	0.13
$CrTe_2$	0.96	0.10	0.34	0	0.53	**$CoTe_2$**	0.37	0	0.58	0.39	0.30
MnS_2	1.17	0.29	0.77	0	2.16	**NiS_2**	0.17	0	0.74	0.88	1.83
$MnSe_2$	0.90	0.08	0.28	0	1.47	**$NiSe_2$**	0.18	0	0.35	0.68	1.18
$MnTe_2$	0.21	0	0.15	0.41	1.07	**$NiTe_2$**	0.04	0	0.43	0.70	0.89

Table S2. The optimized lattice constant (L, Å), and formation energy (E_f, eV/atom) of TMD chains. The E_f of H-phase and T-phase TMD monolayers were computed for comparison.

TMD	L	E_f			TMD	L	E_f		
		Chain	H	T			Chain	H	T
ScS_2	3.67	-1.13	-1.16	-1.24	MnS_2	5.23	-0.41	-0.46	-0.56
$ScSe_2$	3.82	-1.02	-0.99	-1.17	$MnSe_2$	5.41	-0.23	-0.34	-0.47
$ScTe_2$	4.09	-0.53	-0.61	-0.75	$MnTe_2$	3.77	0.01	-0.13	-0.22
TiS_2	6.17	-1.09	-1.16	-1.31	FeS_2	5.13	-0.26	-0.32	-0.37
$TiSe_2$	6.37	-0.89	-1.01	-1.13	$FeSe_2$	5.34	-0.15	-0.27	-0.31
$TiTe_2$	6.72	-0.42	-0.61	-0.71	$FeTe_2$	3.58	0.07	-0.09	-0.11
VS_2	5.71	-0.76	-0.91	-0.90	CoS_2	3.19	-0.18	-0.22	-0.33
VSe_2	5.90	-0.58	-0.74	-0.68	$CoSe_2$	3.32	-0.11	-0.22	-0.32
VTe_2	6.19	-0.15	-0.35	-0.09	$CoTe_2$	3.55	0.02	-0.15	-0.23
CrS_2	5.32	-0.45	-0.66	-0.52	NiS_2	3.30	-0.13	-0.17	-0.31
$CrSe_2$	5.49	-0.27	-0.47	-0.43	$NiSe_2$	3.40	-0.11	-0.17	-0.33
$CrTe_2$	5.86	0.16	-0.08	-0.16	$NiTe_2$	3.61	0.07	-0.05	-0.14

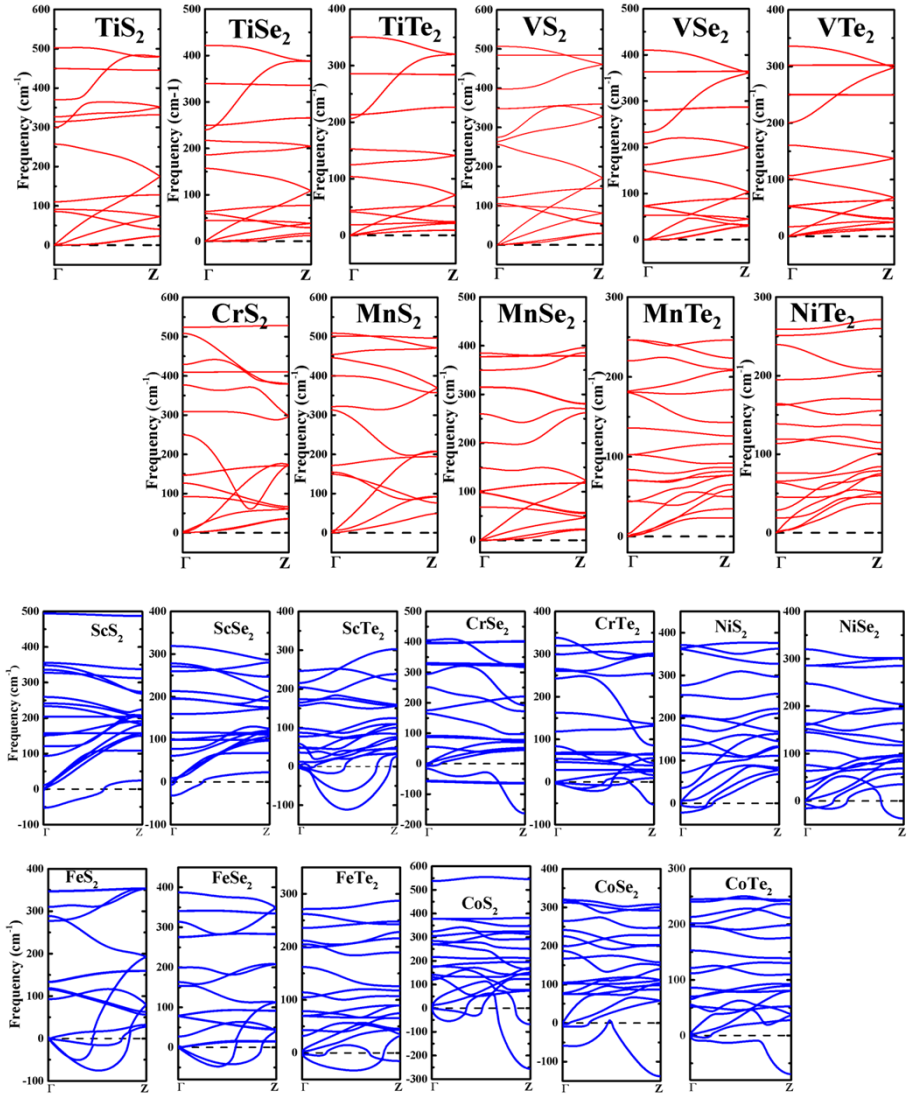

Figure S1. The calculated phonon dispersion spectra of MX_2 chains.

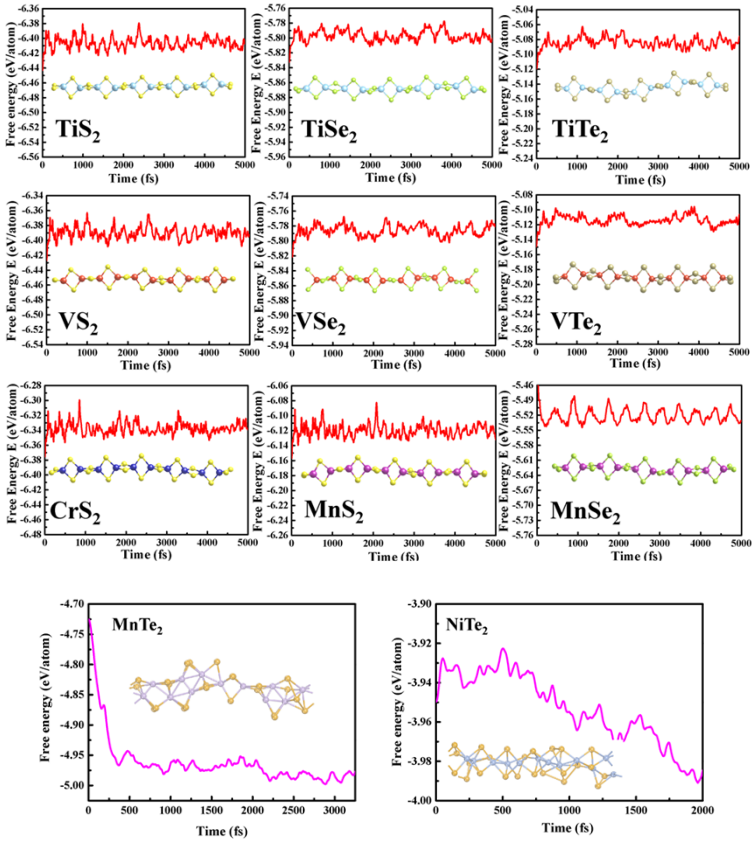

Figure S2. AIMD evolutions of total energy per atoms during simulations. The inset show the snapshot of MX_2 chains at 300K after simulations.

Table S3. The lattice parameters and atomic coordinates of nanowires.

Nanowire	TiS_2	$TiSe_2$	$TiTe_2$	VS_2	VSe_2
Lattice $\alpha=\beta=\gamma=90°$	$a = b = 25$ Å $c = 6.17$ Å	$a = b = 25$ Å $c = 6.38$ Å	$a = b = 25$ Å $c = 6.72$Å	$a = b = 25$ Å $c = 5.71$ Å	$a = b = 25$ Å $c = 5.90$ Å
Atomic coordinates	Ti(0.5 0.5 0.25)	Ti(0.5 0.5 0.25)	Ti(0.5 0.5 0.25)	V(0.5 0.5 0.25)	V(0.5 0.5 0.25)
	Ti(0.5 0.5 0.75)	Ti(0.5 0.5 0.75)	Ti(0.5 0.5 0.75)	V(0.5 0.5 0.75)	V(0.5 0.5 0.75)
	S(0.567 0.5 0.0)	Se(0.573 0.5 0.0)	Te(0.581 0.5 0.0)	S(0.568 0.5 0.0)	Se(0.573 0.5 0.0)
	S(0.433 0.5 0.0)	Se(0.427 0.5 0.0)	Te(0.419 0.5 0.0)	S(0.432 0.5 0.0)	Se(0.427 0.5 0.0)
	S(0.5 0.433 0.5)	Se(0.5 0.427 0.5)	Te(0.5 0.419 0.5)	S(0.5 0.432 0.5)	Se(0.5 0.427 0.5)
	S(0.5 0.567 0.5)	Se(0.5 0.573 0.5)	Te(0.5 0.581 0.5)	S(0.5 0.568 0.5)	Se(0.5 0.573 0.5)
Nanowire	VTe_2	CrS_2	MnS_2	$MnSe_2$	
Lattice $\alpha=\beta=\gamma=90°$	$a = b = 25$ Å $c = 6.19$ Å	$a = b = 25$ Å $c = 5.32$ Å	$a = b = 25$ Å $c = 5.23$ Å	$a = b = 25$ Å $c = 5.41$ Å	
Atomic coordinates	V(0.5 0.5 0.25)	Cr(0.5 0.5 0.25)	Mn(0.5 0.5 0.25)	Mn(0.5 0.5 0.25)	
	V(0.5 0.5 0.75)	Cr(0.5 0.5 0.75)	Mn(0.5 0.5 0.75)	Mn(0.5 0.5 0.75)	
	Te(0.581 0.5 0.0)	S (0.567 0.5 0.0)	S(0.566 0.5 0.0)	Se(0.571 0.5 0.0)	
	Te(0.419 0.5 0.0)	S(0.433 0.5 0.0)	S(0.434 0.5 0.0)	Se(0.429 0.5 0.0)	
	Te(0.5 0.419 0.5)	S(0.5 0.433 0.5)	S(0.5 0.434 0.5)	Se(0.5 0.429 0.5)	
	Te(0.5 0.581 0.5)	S(0.5 0.567 0.5)	S(0.5 0.566 0.5)	Se(0.5 0.571 0.5)	

Table S4. The formation energies of 1D nanowires with different stoichiometric ratio.

Composition	M:X			Composition	M:X		
	1:2	1:1 (Ref[1])	1:3 (Ref[2])		1:2	1:1 (Ref[1])	1:3 (Ref[2])
ScS	-1.13	-1.52	/	**MnS**	-0.41	0.24	/
ScSe	-1.02	-1.34	/	**MnSe**	-0.23	0.36	/
ScTe	-0.53	-0.95	/	**MnTe**	0.01	0.61	/
TiS	-1.09	-1.14	-1.04	**FeS**	-0.26	-0.35	/
TiSe	-0.89	-0.95	-0.83	**FeSe**	-0.15	-0.26	/
TiTe	-0.42	-0.57	-0.51	**FeTe**	0.07	/	/
VS	-0.76	-0.78	-0.65	**CoS**	-0.18	-0.27	/
VSe	-0.58	-0.61	-0.46	**CoSe**	-0.11	-0.20	/
VTe	-0.15	-0.31	-0.16	**CoTe**	0.02	-0.05	/
CrS	-0.45	-0.55	/	**NiS**	-0.13	-0.31	/
CrSe	-0.27	-0.41	/	**NiSe**	-0.11	-0.25	/
CrTe	0.16	-0.17	/	**NiTe**	0.07	-0.13	/

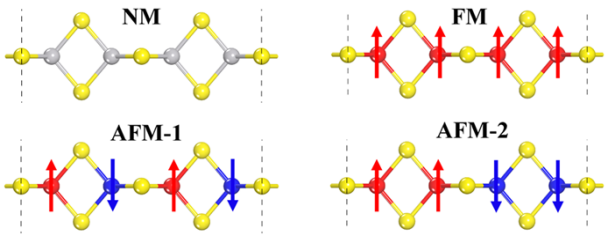

Figure S3. Various spin configurations including nonmagnetic (NM), ferromagnetic (FM) and two anti-ferromagnetic (AFM) states. The majority spin and minority spin on the metal atoms are represented by red and blue arrows, respectively.

Table S5. The relative energies (meV/M) between FM, NM, and AFM states.

Chain	NM		AFM-1		AFM-2		G.S	
	PBE	**HSE06**	**PBE**	**HSE06**	**PBE**	**HSE06**	**PBE**	**HSE06**
VS_2	244	558	210	170	147	311	FM	FM
VSe_2	218	546	196	257	155	342	FM	FM
VTe_2	208	776	189	426	170	232	FM	FM
CrS_2	11	184	10	62	12	165	FM	FM
MnS_2	-213	444	-224	-540	-154	-283	AFM-1	AFM-1
$MnSe_2$	39	596	-8	-709	36	-323	AFM-1	AFM-1

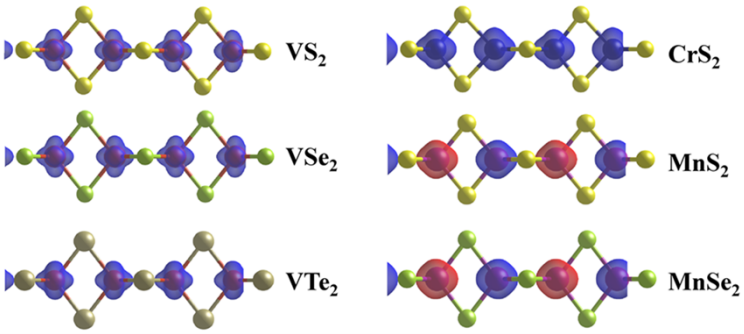

Figure S4. Lateral views of spin charge density distribution on MX_2 chains with an isovalue of 0.02 e/Bohr^3. The majority and minority spin densities are shaded in blue and red colors, respectively.

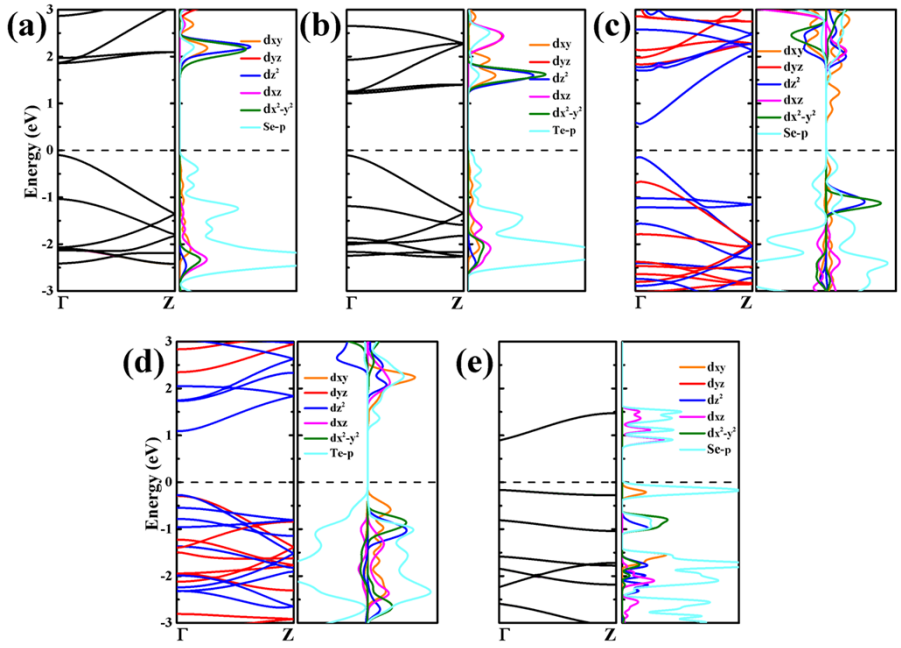

Figure S5. The projected band structures and density of states of (a) $TiSe_2$, (b) $TiTe_2$, (c) VSe_2, (d) VTe_2 and (e) $MnSe_2$ chains.

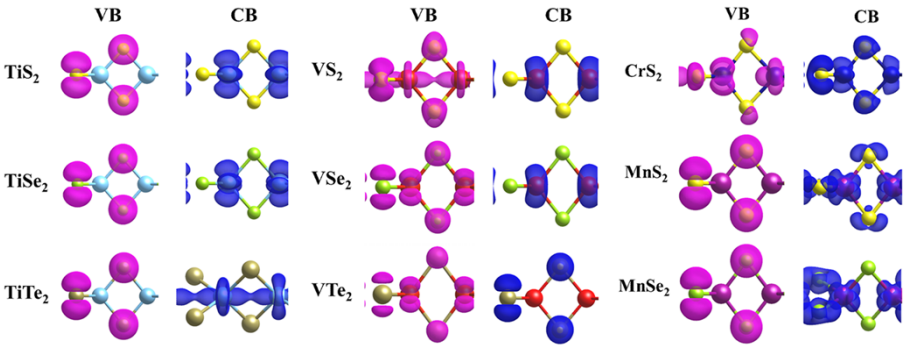

Figure S6. The partial charge density of the valence band maximum (VBM) and conduction band minimum (CBM) for MX_2 atomic chains are plotted by purple and blue colors with an isovalue of 5×10^{-3}.

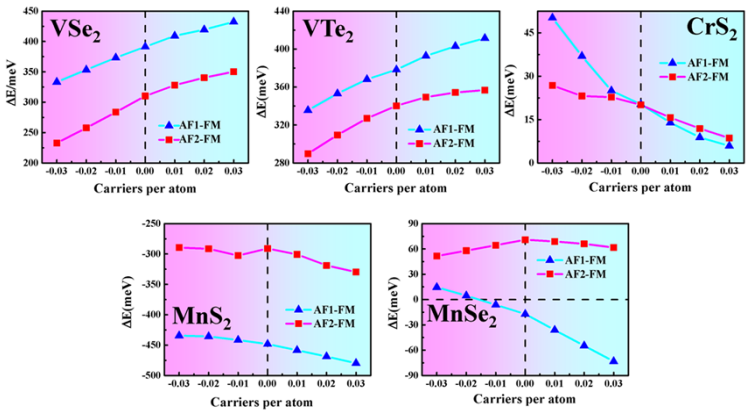

Figure S7. The energy difference between AFM and FM states of MX_2 chains with carrier injection.

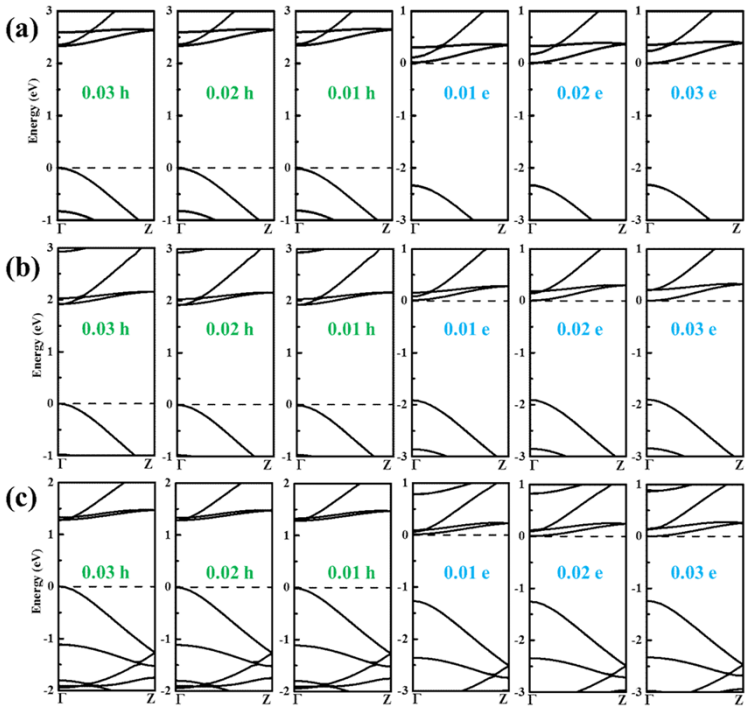

Figure S8. The band structures of (a) TiS_2, (b) $TiSe_2$, and (c) $TiTe_2$ chains with carrier injection.

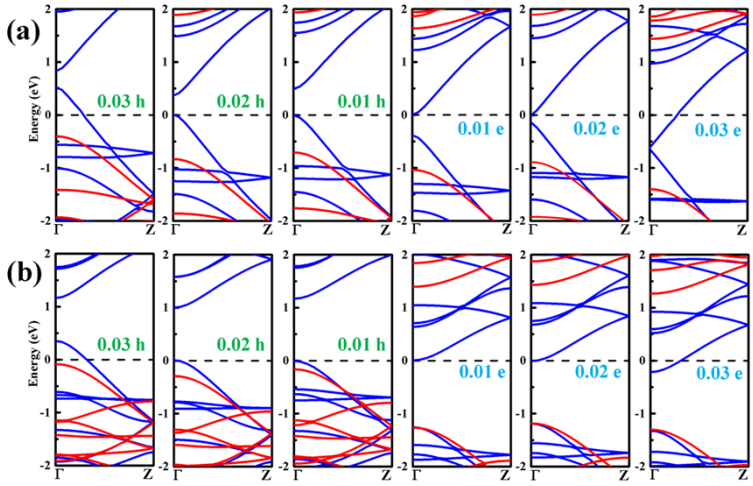

Figure S9. The band structures of (a) VSe_2 and (b) VTe_2 chains with carrier injection.

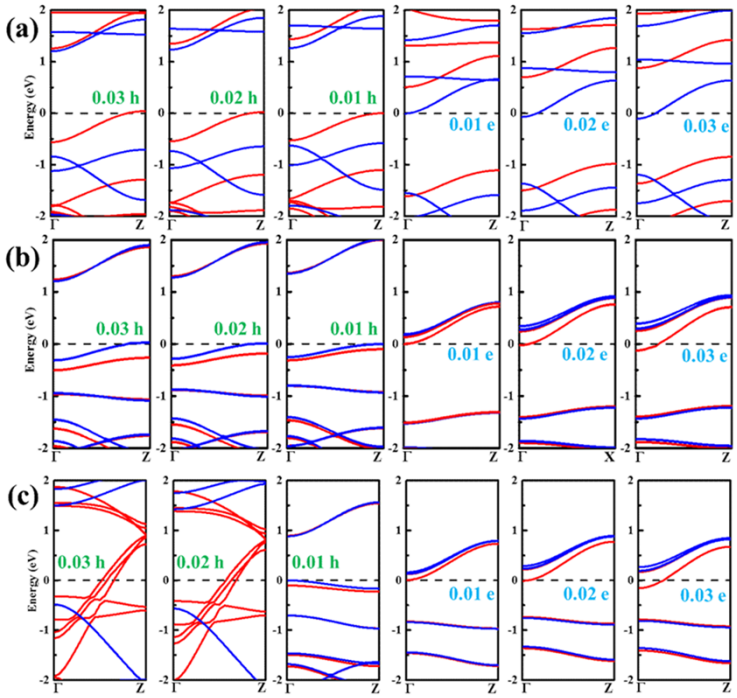

Figure S10. The band structures of (a) CrS_2, (b) MnS_2, and (c) $MnSe_2$ chains with carrier injection.

Table S6. Calculated magnetic anisotropy energy (μeV/metal) of MX_2 chains. EA refers to the easy magnetization axis.

Chain	E[001] - E[100]	EA
VS_2	-51.7	[001]
VSe_2	-588.4	[001]
VTe_2	-3784.2	[001]
CrS_2	19.0	[100]
MnS_2	122.1	[100]
$MnSe_2$	-807.1	[001]

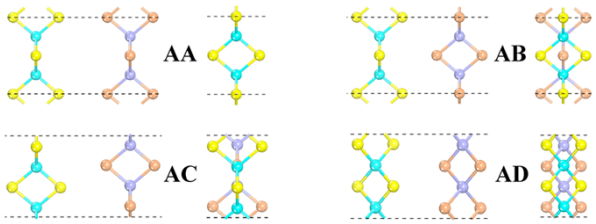

Figure S11. The four types of inter-chain stacking configurations. The top and side views are displayed in left and right panels, respectively. The adjacent chain is shown with different colors.

Table S7. The calculated total energies (eV/metal), inter-chain coupling energy ($E_c = E_{bundle} - 2E_{chain}$, meV/metal) and energy difference between inter-chain FM and inter-chain AFM states ($\Delta E = E_{AFM} - E_{FM}$, meV/metal).

	AA-stacking		**AB-stacking**		**AC-stacking**		**AD-stacking**		**□E**	
	FM	**AFM**	**FM**	**AFM**	**FM**	**AFM**	**FM**	**AFM**	**Ec**	**ΔE**
VS_2	-78.499	-78.498	-78.601	-78.612	-78.530	-78.528	-78.612	-78.613	-166	-0.3
VSe_2	-71.468	-71.466	-71.589	-71.597	-71.505	-71.506	-71.614	-71.697	-232	-20.6
VTe_2	-63.651	-63.652	-63.810	-63.823	-63.816	-63.704	-64.000	-63.891	-318	27.3
CrS_2	-77.169	-77.162	-77.303	-77.293	-77.210	-77.301	-77.394	-77.452	-256	-14.4

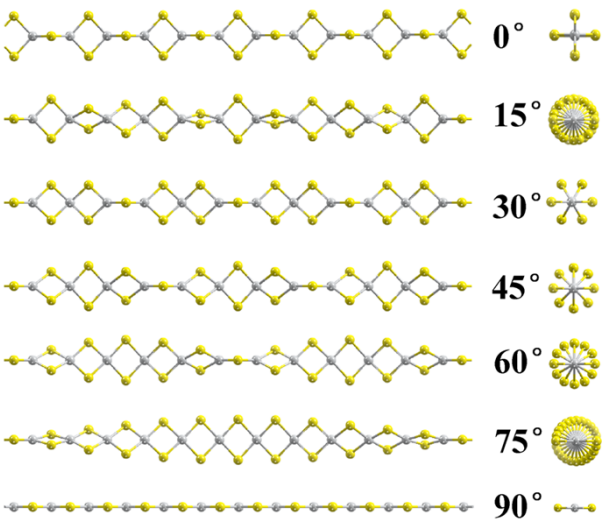

Figure S12. Atomic structures of twisted single chain TiS_2 nanowires. The side and front views are shown in left and right panels, respectively.

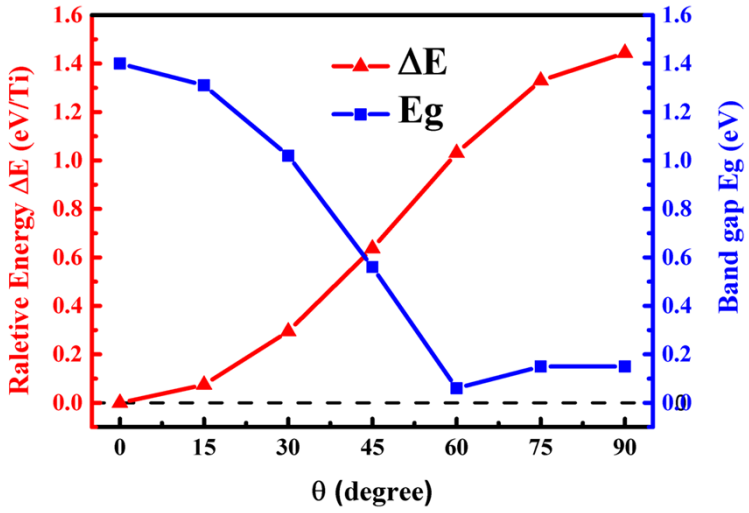

Figure S13. Variation of the total energy per metal and energy gap of twisted TiS_2 nanowire with the rotation angle.

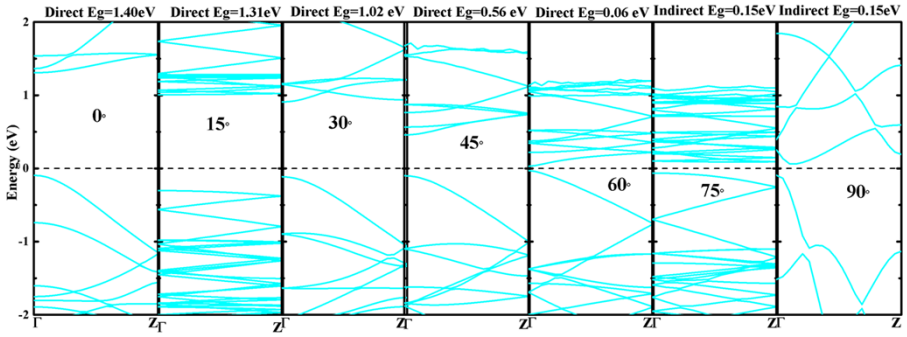

Figure S14. The band structure of twisted TiS_2 nanowire with different rotation angle at PBE level.

Table S8. The unit cell lattice constant L (Å) of chain and CNT, the supercells of chains (m) and CNT (n) used to construct heterostructures, and the lattice mismatch between chain and CNT. The "+" and "-" represent tensile and compressive strains, respectively.

CNT@Chain	Chain	CNT	Supercell	Mismatch
	L	L	(Chain) m : n (CNT)	(%)
TiS_2	6.17	2.46	2:5	+0.4
$TiSe_2$	6.37	2.46	2:5	+3.7
$TiTe_2$	6.72	2.46	3:8	+2.4
VS_2	5.71	2.46	3:7	-0.4
VSe_2	5.90	2.46	3:7	+2.9
VTe_2	6.19	2.46	2:5	+0.6
CrS_2	5.32	2.46	4:9	-3.9
MnS_2	5.23	2.46	4:9	-5.5
$MnSe_2$	5.41	2.46	4:9	-2.2

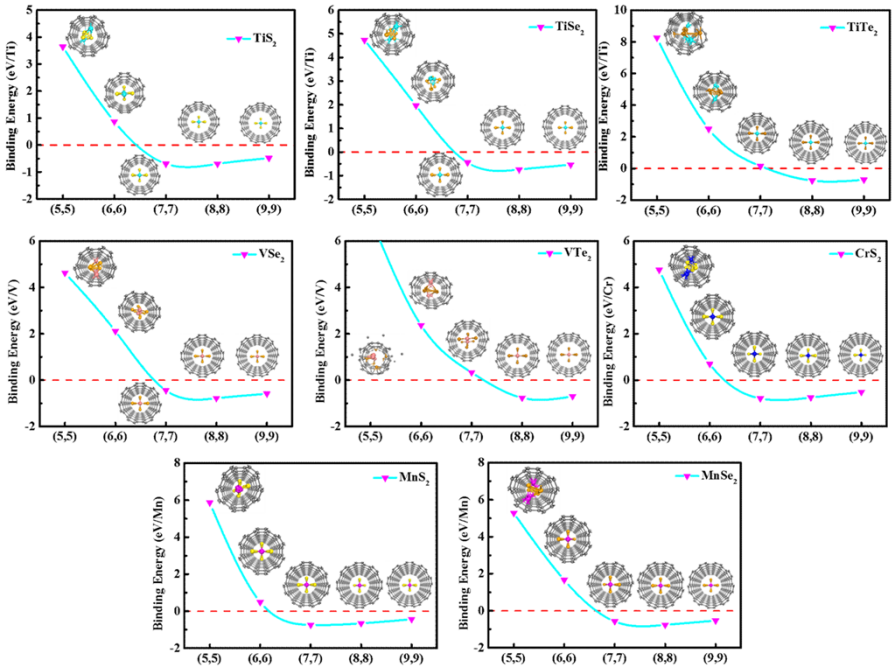

Figure S15. The evolution of binding energy with diameter of CNT. The inset shows front views of MX_2 chains embedded in CNT.

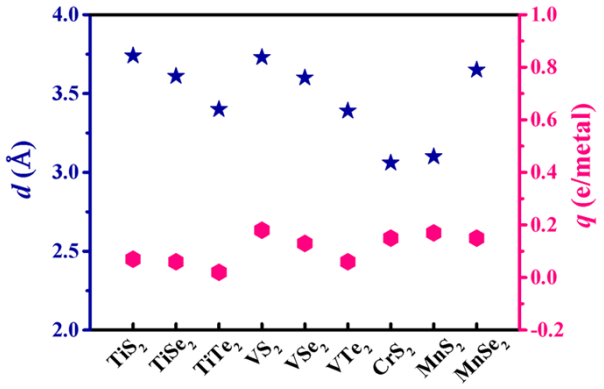

Figure S16. The separation ***d*** between chain and CNT, and charge transfer ***q*** (*e*/metal) from CNT to chain.

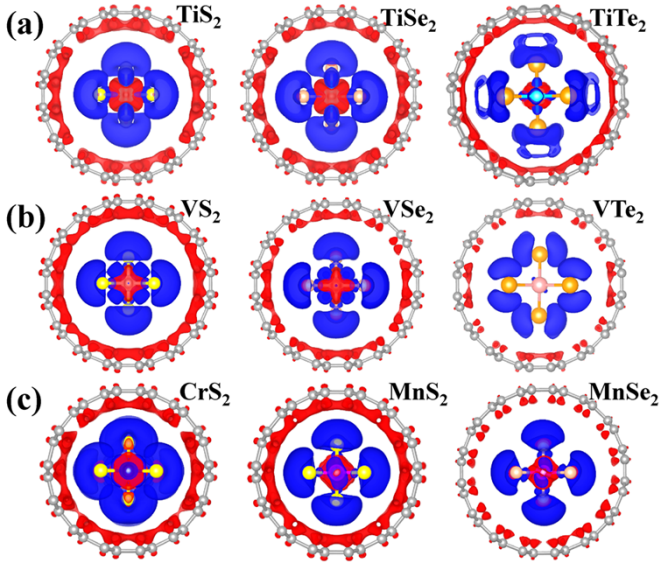

Figure S17. Electron density transferred from the CNT to the inside MX_2 chains. Isovalues are set as 2×10^{-4}, 4×10^{-4}, and 5×10^{-4} e/Bohr^3 for (a) TiX_2, (b) VX_2, and (c) MnX_2 single-chain embedded inside CNT. Electron accumulation and depletion are shaded in blue and red, respectively.

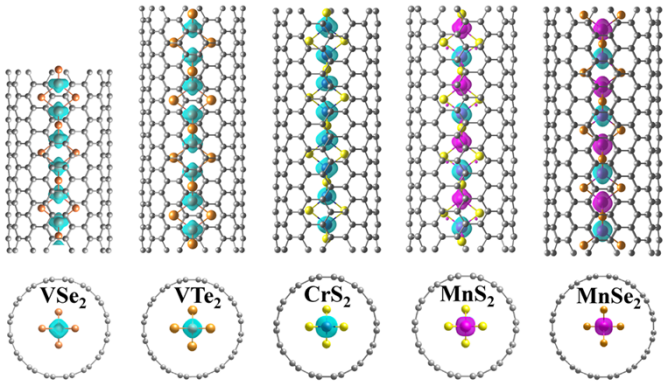

Figure S18. The spin charge density distribution in joint system. The majority and minority spin charge density are displayed in cyan and purple, respectively.

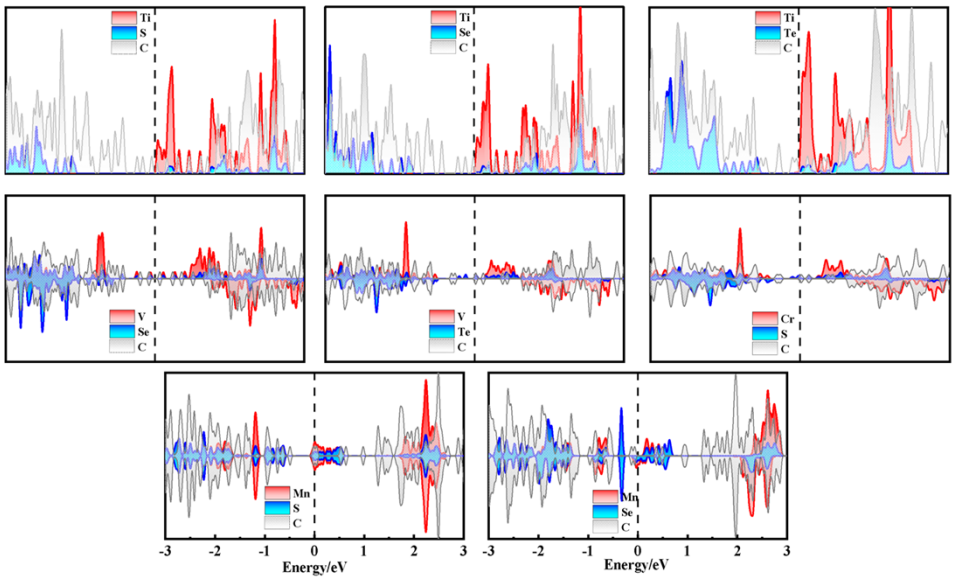

Figure S19. The projected density of states of MX_2 chains encapsulated inside CNT.

Reference:

1. C. Shang, L. Fu, S. Zhou and J. Zhao, *JACS Au*, 2021, **1**, 147-155.
2. S. Stonemeyer, J. D. Cain, S. Oh, A. Azizi, M. Elasha, M. Thiel, C. Song, P. Ercius, M. L. Cohen and A. Zettl, *Journal of the American Chemical Society*, 2021, **143**, 4563-4568.